Applied Catalysis B: Environmental 196 (2016) 108–116

Contents lists available at ScienceDirect

Applied Catalysis B: Environmental

journal homepage: www.elsevier.com/locate/apcatb

A novel W-doped Ni-Mg mixed oxide catalyst for CO_2 methanation

Yong Yan[a], Yihu Dai[a], Hong He[b,c], Yunbo Yu[b,c,**], Yanhui Yang[a,*]

[a] School of Chemical and Biomedical Engineering, Nanyang Technological University, Singapore, 637459, Singapore
[b] State Key Joint Laboratory of Environment Simulation and Pollution Control, Research Center for Eco-Environmental Sciences, Chinese Academy of Sciences, Beijing, 100085, China
[c] CAS Center for Excellence in Urban Atmospheric Environment, Chinese Academy of Sciences, Xiamen, 361021, China

ARTICLE INFO

Article history:
Received 24 November 2015
Received in revised form 8 May 2016
Accepted 9 May 2016
Available online 10 May 2016

Keywords:
CO_2 methanation
Ni-W-Mg mixed oxide
Ni-Mg interactions
Monodentate formate

ABSTRACT

Novel Ni-W-Mg mixed oxide catalysts ($NiWMgO_x$) were prepared by homogeneous precipitation and attempted for the methanation of CO_2. Adding W remarkably promoted the activity with improved stability, anti-CO-poisoning ability and resistance against coke formation compared to the undoped $NiMgO_x$ catalyst. The superior reactivity of monodentate formate towards hydrogenation than that of bidentate formate species was identified by DRIFTS analysis and the formation of more active monodentate formate species was indisputably facilitated by W additives, leading to the greatly enhanced catalytic activity. H_2-TPR and CO_2-TPD characterization showed that doping W increased the number of stable CO_2 adsorption sites and helped in anchoring the Ni sites as a result of strengthened Ni-Mg interaction, both of which were responsible for the enhanced CO_2 methanation activity and the improved resistance against sintering.

1. Introduction

The methanation of CO_2 casts a direction to recycle the atmospheric C and subsequently reduces the greenhouse gas effect. Several efforts have been devoted to the development of effective and stable catalysts for this particular reaction since early 20th century [1,2]. Supported noble metal catalysts, such as Ru [3–5], Rh [6–9] and Pd [10–12] are well known for their excellent activity and stability in CO_2 methanation under relatively mild reaction conditions. Nevertheless, the large-scale application of these catalysts has been limited by their high cost. As an alternative solution, non-noble transition metal catalysts (*e.g.*, Ni, Co) have attracted increasing attention for their comparable methanation activity with highly improved cost-efficiency [13–16].

The challenge of using Ni-based catalysts in CO_2 methanation is to improve the low-temperature activity, not only for the purpose of energy saving, but also for the reason that high temperature reaction is limited by the chemical equilibrium. Applying novel support materials such as metal-organic frameworks (MOFs) is one of the solutions, which can greatly improve the low-temperature performance for Ni-based catalysts [17]. However, the conventional metal oxides remain as the most promising support to optimize Ni-based catalysts for CO_2 methanation because of their high thermal stability and low cost [18]. Among those, MgO shows the potential because the strong interaction between Ni species and MgO favors the formation of highly dispersed small Ni particles, which contributes to the great enhancement of CO_2 methanation activities [13,16,19,20]. Further modifications of the surface properties can be achieved by controlling the formation of 'ideal' Ni-Mg solid solution [21,22]. Ni-MgO nanoparticles encapsulated by porous silica shell, reveals a remarkable improvement in CO_2 conversion with high stability compared to the encapsulated NiO without MgO [23]. To the contrary, the presence of MgO is considered to lower the methanation activity due to the poor reducibility of Ni-Mg solid solution [24]. These two apparently contradictory results indicate that the fine-tuning of the interaction between Ni species and MgO support plays an essential role in optimizing the performance of Ni-Mg catalysts for CO_2 methanation.

On the other hand, improvement of the long-term stability of Ni-based catalysts in CO_2 methanation at high temperature requires more efforts. The deactivation of catalysts by coke formation and sintering of metal particles is accelerated when a large amount of heat is released as the exothermal reaction further proceeds [16,24,25]. Besides, the poison effect of CO *via* the formation and the migration of mobile $Ni(CO)_4$ species on catalyst surface during the methanation reaction cannot be ruled out [15,26]. Nevertheless, several researchers substantiated that the formation of Ni-Mg

* Corresponding author.
** Corresponding author at: State Key Joint Laboratory of Environment Simulation and Pollution Control, Research Center for Eco-Environmental Sciences, Chinese Academy of Sciences, Beijing, 100085, China.
E-mail addresses: ybyu@rcees.ac.cn (Y. Yu), yanhui.yang@live.com, yhyang@ntu.edu.sg (Y. Yang).

http://dx.doi.org/10.1016/j.apcatb.2016.05.016
0926-3373/

solid solution was beneficial for the resistance against deactivation over MgO supported Ni catalysts [20]. For instance, there are two types of NiO species in MgO doped Ni/Al_2O_3 catalyst: the 'free' NiO and highly dispersed NiO species. However, only the latter one can prevent the agglomeration of Ni crystallites and improve the catalytic activity and stability due to the strong interaction between NiO species and MgO additives [27]. Similar results were reported by Wang et al. [28], who synthesized a durable Ni/MgO catalysts for the CO_2 reforming of methane with remarkable resistance to sintering and coking. The stability enhancement over their catalysts was attributed to the 'anchoring' of metallic Ni by surface defects on the support, which were formed at the vicinity of the reduction sites of Ni species located in the Ni-Mg solid solution. Furthermore, the incorporation of a third component, such as Ru [23], Sr [29], Co [30] has been investigated to improve the stability of Ni-based catalysts for CO_2 methanation. Recently, a synergistic effect between Ni and W in mixed Ni-W-Ce oxide catalysts has been reported, which displayed significant effectiveness in minimizing the coke formation and stabilizing the metal particles for ethanol steam reforming [31].

In this study, a series of W-doped Ni-Mg mixed oxide powder catalysts were prepared by a homogeneous precipitation method and attempted in CO_2 methanation. $NiWMgO_x$ with Ni:W:Mg molar ratio being 1:1:1 exhibited both the excellent methanation activity and CH_4 selectivity. The stability test at 400 °C for 100 h revealed only a negligible activity loss for $NiWMgO_x$. The promotion effect of adding W to the Ni-Mg mixed oxide catalyst was further investigated by *in situ* DRIFTS, CO_2-TPD and H_2-TPR.

2. Experimental

2.1. Catalyst preparation and activity test

During a typical procedure for the homogenous precipitation preparation, desired amounts of $(NH_4)_{10}W_{12}O_{41}$, $(NH_4)_6Mo_7O_{24}{\cdot}4H_2O$, $Fe(NO_3)_3{\cdot}9H_2O$, $Co(NO_3)_2{\cdot}6H_2O$, $Mn(NO_3)_2{\cdot}4H_2O$ or $Cu(NO_3)_2{\cdot}3H_2O$ was firstly dissolved in water ($H_2C_2O_4{\cdot}2H_2O$ was applied for dissolving $(NH_4)_{10}W_{12}O_{41}$ and $(NH_4)_6Mo_7O_{24}{\cdot}4H_2O$), followed by mixing with an aqueous solution of $Ni(NO_3)_2{\cdot}6H_2O$ and $Mg(NO_3)_2{\cdot}6H_2O$. Subsequently, excessive urea aqueous solution was added into the mixed solution. The solution was heated to 90 °C and held for 12 h under constant stirring. After filtering and washing with deionized water, the resulting precipitant was dried at 100 °C overnight and calcined at 500 °C for 4 h in air. For comparison, Ni_aMgO_x (a = 0.5, 0.8, 1.0, 1.2) catalyst was also prepared following the same procedure.

Prior to the activity tests, 100 mg of catalyst was in situ reduced in a H_2 gas flow of 30 mL/min at 500 °C for 60 min in a fix-bed quartz tube micro-reactor. The catalytic activity measurements were carried out at atmospheric pressure by passing a gaseous mixture of CO_2 (5%) and H_2 (20%) in He balance at a total flow rate of 100 mL/min (GHSV ~ 40,000 h^{-1}). The inlet and outlet flows were analyzed by an on-line gas chromatograph (Agilent 6890) equipped with both a FID and a TCD detector. The sampling data were collected when reaction reached a steady state (60–120 min after reaching the desired reaction temperature).

2.2. Characterizations

Powder X-ray diffraction (XRD) patterns were recorded on a Bruker Advance 8 X-ray diffractometer using a Ni filtered Cu Kα radiation (λ = 0.154 nm), operated at 40 kV and 40 mA. XRD data were collected between 10 and 90° (2θ) with a resolution of 0.02° (2θ). The N_2 adsorption-desorption isotherms were measured using a Quantachrome Autosorb-1C instrument at liquid N_2 temperature (–196 °C). Prior to the N_2 physisorption, all the catalysts were outgassed at 300 °C for 5 h in vacuum. The specific surface areas were calculated by BET equation at P/P_0 in the partial pressure range of 0.05–0.35. Transmission electron microscope (TEM) images were obtained on a JEOL JEM-2100F which was operated at 200 kV.

In situ DRIFTS experiments were performed on an FTIR spectrometer (Nicolet is-50) equipped with a smart collector and an MCT/A detector cooled by liquid nitrogen. The temperature was controlled precisely by an Omega programmable temperature controller. Prior to each experiment, the sample was pretreated at 500 °C for 60 min in H_2 and then cooled down to 300 °C. The background spectra were collected in flowing Ar and automatically subtracted from the sample spectrum. The gas mixture was controlled as follows: 5% H_2, 20% CO_2 and Ar balance with total flow rate of 200 mL/min. All spectra were recorded by accumulating 100 scans with a resolution of 4 cm^{-1}.

The H_2 chemisorption was carried out on a Quantachrome Automated chemisorption analyzer. Approximately 200 mg of catalyst was reduced in H_2 stream at 500 °C for 60 min, followed by Ar purge at 500 °C for 60 min. Then, the catalysts were cooled down to 30 °C for the H_2 chemisorption measurements. Coke deposits were determined on a PerkinElmer Diamond TG/DTA equipment. The spent catalysts was heated under N_2 stream up to 800 °C with a ramp of 10 °C/min.

CO_2-TPD experiments were performed using a Micromeritics Autochem II 2920 instrument equipped with a TCD detector. Prior to TPD experiments, the samples (100 mg) were pretreated at 500 °C in H_2 for 60 min and cooled down to room temperature. Then the sample was exposed to 20% CO_2/Ar for 60 min, followed by Ar purge for another 60 min. The temperature was raised to 500 °C at a ramp of 10 °C/min and the signals of CO_2 (m/z = 44 for CO_2) were recorded by a quadrupole mass spectrometer (MKS Cirrus).

H_2-TPR measurements for the catalyst samples were conducted on the same instruments as CO_2-TPD. After being pretreated under an air flow in a quartz U-tube reactor at 500 °C for 60 min, the samples were cooled down to room temperature in Ar flow. Then 10% H_2/Ar was introduced to pass through the catalyst bed until a stable TCD signal was observed. Subsequently, a temperature ramping program from room temperature to 1000 °C at rate of 10 °C/min was performed, and the H_2 consumption was monitored by TCD after the removal of H_2O.

3. Results and discussion

3.1. CO_2 methanation activity of catalysts with different Ni/Mg molar ratio

CO_2 conversions over NiO, MgO and Ni_aMgO_x (a = 0.5, 0.8, 1.0, 1.2) catalysts along with reference Ni/MgO(imp) (synthesized with the same metal composition as $Ni_{1.0}MgO_x$) prepared by impregnation method were presented in Fig. 1. $Ni_{0.5}MgO_x$ exhibited a relatively poor activity at temperature lower than 300 °C. Both $Ni_{0.8}MgO_x$ and $Ni_{1.0}MgO_x$ with higher Ni loadings showed enhanced activities towards CO_2 methanation, especially at low temperature. At 300 °C, the CO_2 conversion reached 70% over $Ni_{1.0}MgO_x$ with 99% selectivity to CH_4. As a reference, Ni/MgO(imp) showed a poor CO_2 conversion less than 20% at the same temperature, implying that the homogeneous precipitation preparation method improved the dispersion of active Ni species on Ni-Mg mixed oxide catalysts for CO_2 methanation. However, further increasing Ni loading to Ni/Mg = 1.2 led to a noticeable decrease in CO_2 conversion, possibly due to the aggregation of surface Ni particles [17,32]. Pure NiO and MgO presented a significantly poor activity towards CO_2 methanation together with an inferior

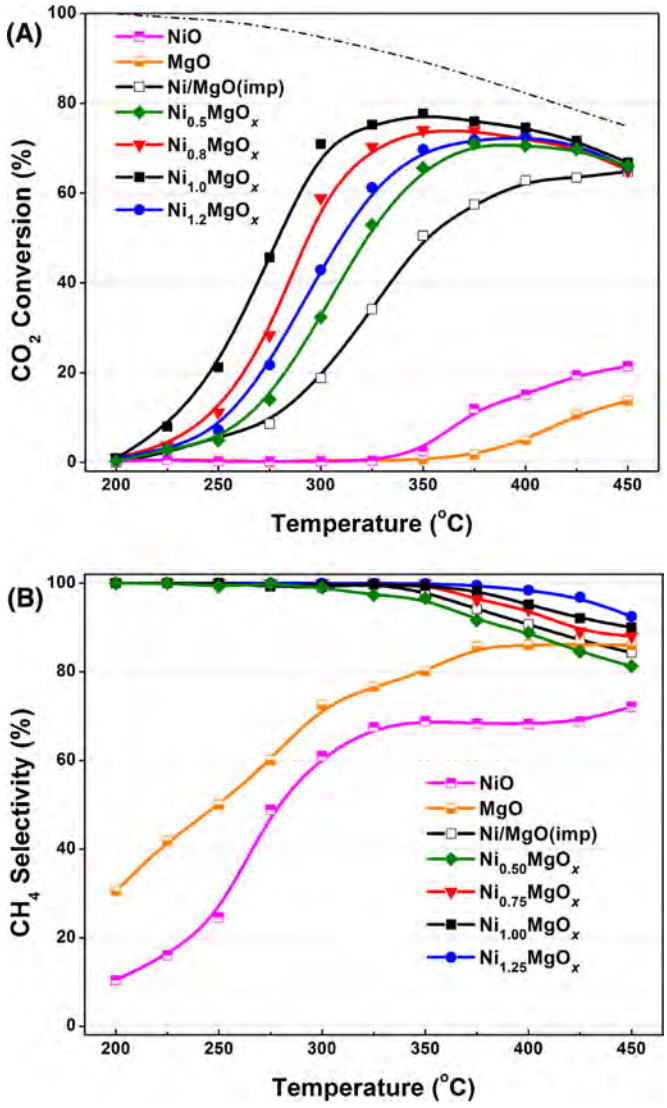

Fig. 1. (A) CO_2 conversion and (B) CH_4 selectivity over catalysts with different Ni: Mg molar ratio. Dashed line – thermodynamic equilibrium conversion values. Conditions: CO_2 5%, H_2 20%, He as balance, GHSV ~ 40,000 h^{-1}.

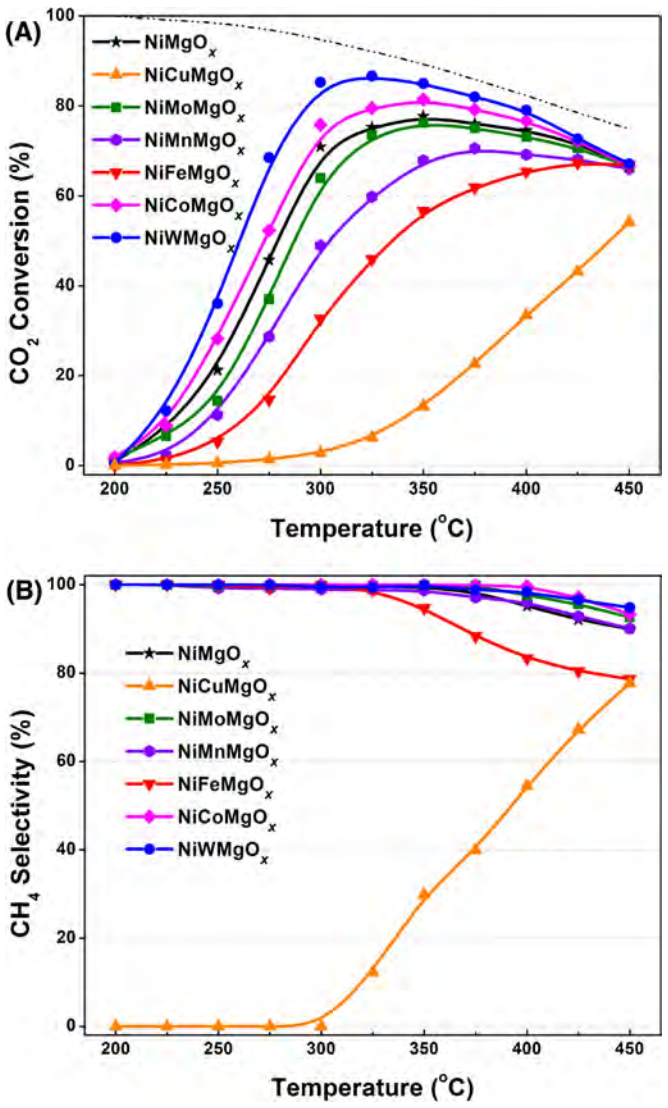

Fig. 2. (A) CO_2 conversion and (B) CH_4 selectivity over $NiMgO_x$ catalysts doped by different transit metals. Dashed line – thermodynamic equilibrium conversion values. Conditions: CO_2 5%, H_2 20%, He as balance, GHSV ~ 40,000 h^{-1}.

selectivity to CH_4, indicating the essential role of the synergetic interaction between Ni and Mg for CO_2 methanation. Based on the activity measurements, the $Ni_{1.0}MgO_x$ was chosen as the catalyst for further optimization.

3.2. CO_2 methanation activity over different transition metal doped catalysts

The $NiMgO_x$ catalysts doped by different transition metals at the molar ratio of 1:1:1 including W, Mo, Fe, Co, Mn and Cu were synthesized by the same homogeneous precipitation method and tested for CO_2 methanation. As shown in Fig. 2, $NiCuMgO_x$ showed an obviously different reaction pattern from other catalysts, with a higher reactivity for reversed water gas shift than methanation of CO_2. The addition of Mo into Ni-Mg mixed oxide resulted in a slight decrease of the low temperature activity. Mn- and Fe-doped catalysts showed a remarkably decreased CO_2 conversion than $NiMgO_x$ and a significant decrease of selectivity to CH_4 was observed over $NiFeMgO_x$. In contrast, Co and W doping resulted in an enhancement of both CO_2 conversion and CH_4 selectivity. The corresponding CO_2 conversions at 300 °C over $NiWMgO_x$ and $NiCoMgO_x$ were 86% and 74% respectively. Compared to the conversion of 70% over undoped $NiMgO_x$ catalysts, a significant improvement of catalytic activity was observed on $NiWMgO_x$, which was worth further discussing.

3.3. Influence of W dopant molar ratio

At the W: Ni molar ratio of 0.50, a slight increase of CO_2 conversion was observed compared to the undoped $NiMgO_x$ (Fig. 3). Further increasing the W molar ratio in Ni-W-Mg to 0.75 and 1.00 improved the catalytic performance for CO_2 conversion. However, an apparent decline of CO_2 methanation activity was observed when the relative W addition ratio was increased to 1.25. Noticeably, the reference $NiWO_x$ catalyst possessed a remarkably inferior activity for CO_2 methanation to $NiWMgO_x$, indicating that W cannot completely replace the role of Mg as the support for Ni catalysts. The maximum CO_2 conversion was attained when W: Ni molar ratio reached 1:1 in Ni-W-Mg oxide catalysts.

3.4. Influence of CO

CO was observed as an impurity for CO_2 in certain sources such as waste gas emission from power plants [33,34], the pres-

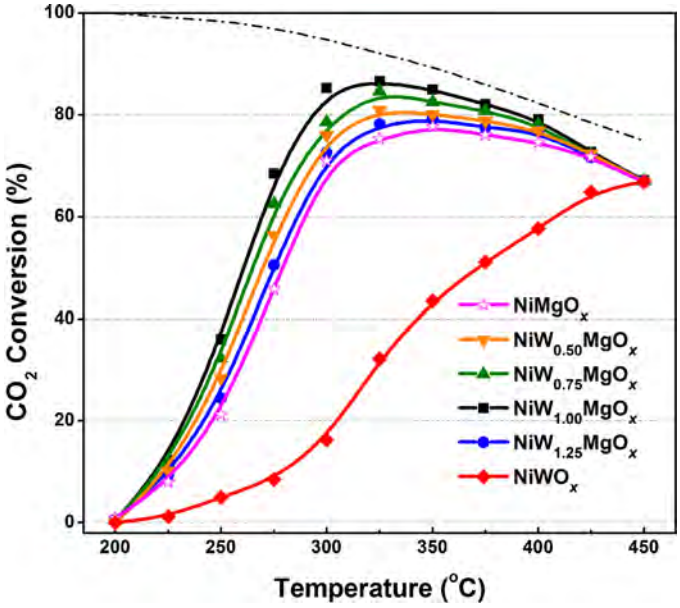

Fig. 3. CO_2 conversion over NiW_bMgO_x (b = 0.50, 0.75, 1.00, 1.25) catalysts. Dashed line – thermodynamic equilibrium conversion values. Conditions: CO_2 5%, H_2 20%, He as balance, GHSV ~ 40,000 h^{-1}.

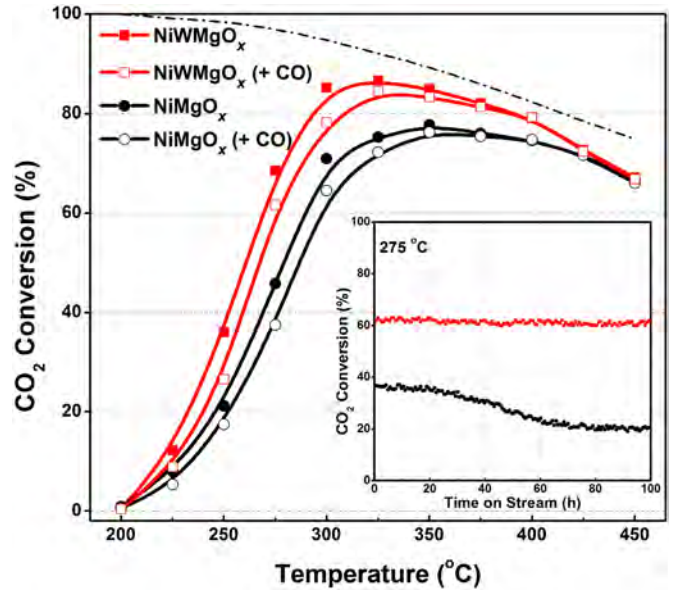

Fig. 4. CO_2 conversion over $NiMgO_x$ and $NiWMgO_x$ in the presence of CO and stability test result (insert). Stability test is ran at 275 °C. Dashed line – thermodynamic equilibrium conversion values. Conditions: CO_2 5%, H_2 23%, CO 1%, He as balance, GHSV ~ 40,000 h^{-1}.

ence of which was reported to inhibit the methanation of CO_2 by strong interaction with the surface of Ni particles [35]. Fig. 4 showed the catalytic activity of $NiMgO_x$ and $NiWMgO_x$ with 1% CO in the gas feeding for CO_2 methanation. A small downshift of CO_2 conversion at temperature lower than 350 °C was found for both catalysts while the high temperature activity remained almost intact, suggesting that the mixed oxide catalysts suffered from confined inhibition effects by the interactions between CO and Ni surface. Apart from the influence mentioned above, the formation of mobile Ni carbonyl species and subsequently growth of Ni particles at low temperature by the facilitation of CO was also the main cause for the deactivation of Ni-based catalysts [15]. Thus, the long-term performances of both samples in the presence

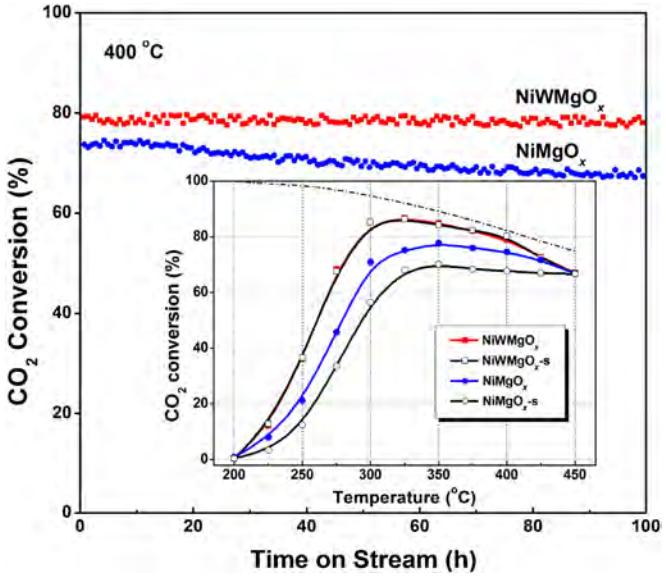

Fig. 5. Stability test result of $NiMgO_x$ and $NiWMgO_x$ catalysts, with activity comparison between spent catalysts after 100 h on stream and fresh catalysts (insert). Dashed line – thermodynamic equilibrium conversion values. Conditions: 400 °C, CO_2 5%, H_2 20%, He as balance, GHSV ~ 40,000 h^{-1}.

of 1% CO were studied at 275 °C for 100 h. CO addition resulted in an immediate decrease of approximately 6% in CO_2 conversion over both $NiMgO_x$ and $NiWMgO_x$, 45% to 38% and 67% to 61% respectively, a consequence of the competitive adsorption of CO. Nonetheless, after exposing to CO-containing reaction gas for 80 h, the CO_2 conversion over $NiMgO_x$ drastically decreased from 38% to 22%, while $NiWMgO_x$ showed almost no deactivation with CO_2 conversion remaining above 60% for up to 100 h. The fact that $NiWMgO_x$ demonstrated excellent activity and anti-CO-poisoning ability indicated $NiWMgO_x$ was also of great promise in applications for methanation of CO_2 from realistic CO-containing sources.

3.5. *Catalysts stability*

The primary obstacle to the application of Ni-based catalysts for methanation is the deactivation at high temperature as a result of sintering of active species. Thus, both $NiMgO_x$ and $NiWMgO_x$ were tested at 400 °C in the same reaction gas used above for 100 h. Prior to the stability test, the catalyst was also *in situ* reduced at 500 °C under H_2 stream for 60 min. As shown in Fig. 5, no activity loss occurred for $NiWMgO_x$ during the long-term test at 400 °C and the selectivity remained at around 98%. In contrast, a decrease in CO_2 conversion from 78% to 68% was observed over $NiMgO_x$. After the stability test, the CO_2 methanation activities of the spent catalysts, denoted as $NiMgO_x$-s and $NiWMgO_x$-s, were subsequently tested repeatedly (as displayed in Fig. 5). No obvious change of CO_2 conversion over $NiWMgO_x$-s was inspected at each temperature point compared to the freshly prepared catalyst, while $NiMgO_x$-s demonstrated a significant activity loss in contrast to the fresh $NiMgO_x$. These results indicated that doping W greatly enhanced the stability of Ni-Mg mixed oxide catalyst, the reasons of which will be further discussed below.

3.6. In situ *DRIFTS study*

The surface intermediates during CO_2 methanation over $NiMgO_x$ and $NiWMgO_x$ were studied by *in situ* DRIFTS at 300 °C. As presented in Fig. 6, the most predominant bands formed were the sharp peak at 1603 cm^{-1} and the broad one centered at 1511 cm^{-1} after passing H_2 and CO_2 for 60 min over $NiMgO_x$. It also

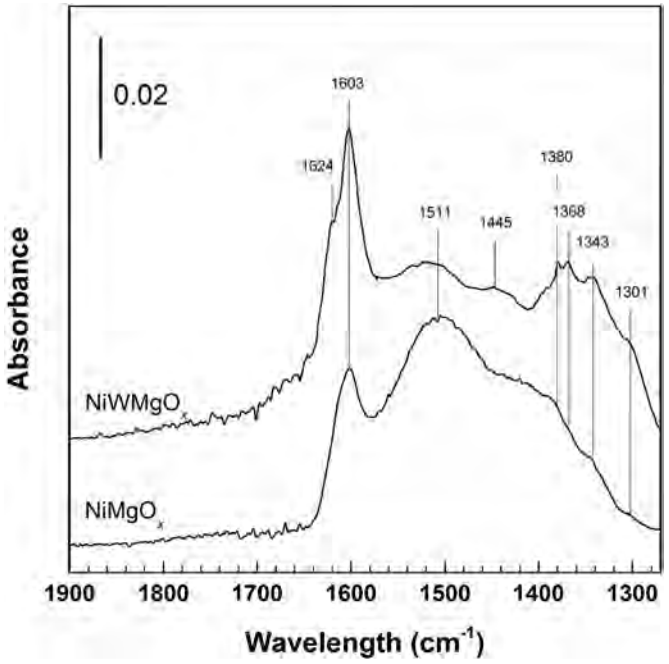

Fig. 6. *In situ* DRIFTS of CO_2 methanation ($CO_2 + H_2$) at 300 °C.

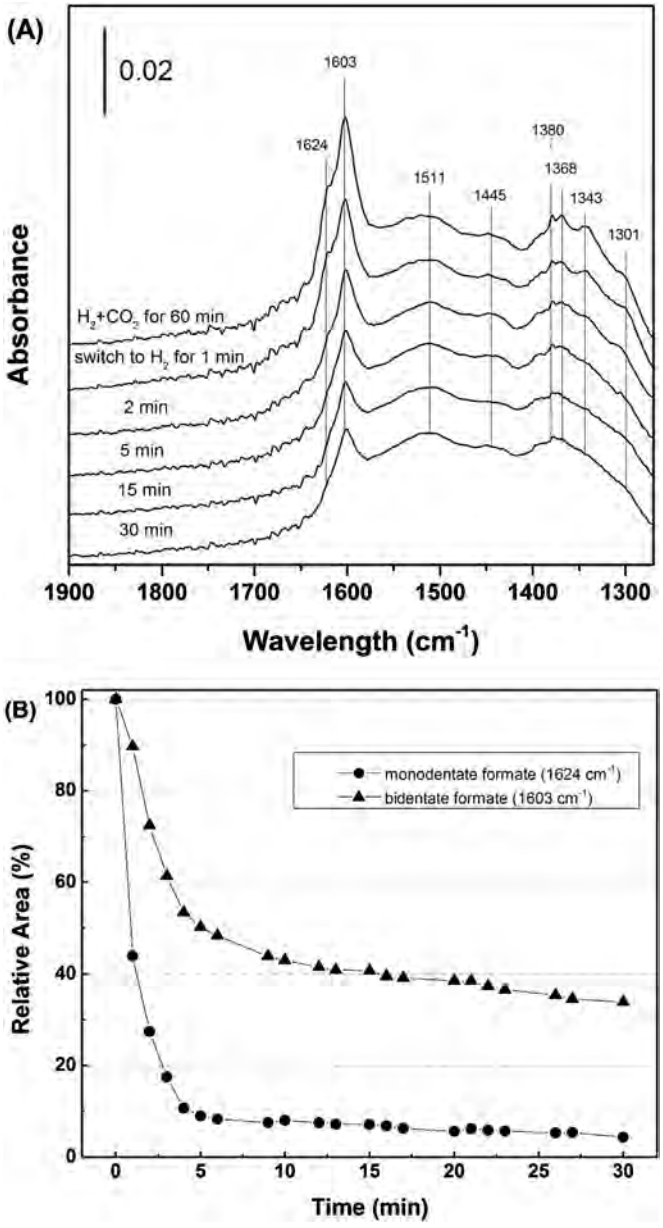

Fig. 7. (A) Dynamic changes of *in situ* DRIFTS spectra over $NiWMgO_x$ as a function of time in a flow of H_2 at 300 °C after being exposed to a flow of $CO_2 + H_2$ for 60 min at 300 °C. (B) Time dependence of the relative peak area ratio to the initial peak area of monodentate formate and bidentate formate species.

should be noted that two shoulder peaks at 1368 and 1343 cm^{-1} were observed on top of the large hump centered at 1380 cm^{-1}. The appearance of characteristic bands of methane at 1301 and 3010 cm^{-1} (results not shown) were in good accordance with the excellent activity. Introduction of CO_2 and H_2 to $NiWMgO_x$ for 60 min resulted in the appearance of another new shoulder peak at 1624 cm^{-1} in addition to those peaks mentioned above, which was probably too weak to be observed over $NiMgO_x$ as it was covered by the strong peak at 1603 cm^{-1}. In addition, evidently stronger bands at 1603 and 1368 cm^{-1} were observed over $NiWMgO_x$ than those on undoped $NiMgO_x$.

Several formate and carbonate species were observed over Ni-based catalysts in the DRIFTS spectra between 1700 and 1200 cm^{-1} during the methanation of CO_2 [34,36,37]. For formate species over Ni-based catalysts, the adsorption configuration is distinguished by the frequency difference ($\Delta\nu$) between ν_s(OCO) and ν_{as}(OCO). A $\Delta\nu$ larger than 250 cm^{-1} often indicated the formation of monodentate configuration, while a $\Delta\nu$ less than or close to 250 cm^{-1} was ascribed to the bidentate formate species [32,37,38]. Thus, in this study, the bands at 1624 and 1343 cm^{-1} were assigned to the ν_s(OCO) and ν_{as}(OCO) of monodentate formate species and the bands at 1603 and 1368 cm^{-1} were ascribed to the bidentate formate species, correspondingly. For the assignment of the bands at 1511, 1445 and 1380 cm^{-1}, different kinds of carbonates have been proposed, including monodentate carbonate [39], bidentate carbonate [36,37] and tridentate carbonate [40]. In the presence of H_2, carbonates can be hydrogenated into formate species and further participated in the methane production [11,34]. Also the direct decomposition of carbonates has been proposed in this process, resulting in the possible formation of CO besides from CO_2, which then followed the reaction pathway of the methanation of CO to yield methane [41]. However, no observance of CO(ads) in our study suggested that the CO_2 methanation reaction pathway over $NiWMgO_x$ involved the hydrogenation of carbonates species into formate species other than the direct decomposition of carbonates [42,43]. Similar reaction pathway has also been reported for Pd-Mg/SiO_2 [11], NiUSY zeolites [34] and Ni/$Ce_{0.5}Zr_{0.5}O_2$ [36]. Thus, the carbonates species can serve as the precursors for the formate species during methanation of CO_2. As key intermediates for CO_2 methanation, the reactivity of different formate species was studied by several groups. Pan et al. [36,37] recently found that the monodentate formate species reacted more rapidly with H_2 than the bidentate formate species and further contributed to the enhanced CO_2 methanation activity. Inspired by this, in this study, we will focus on the role of formate species, which is derived from the hydrogenation of active carbonates in the methanation of CO_2. Thus these three peaks at 1511, 1445 and 1380 cm^{-1} were generally ascribed to the carbonates family.

To obtain the reactivities of these surface species towards H_2 over $NiWMgO_x$, the reaction gas was switched to 20% H_2/Ar after exposure to $CO_2 + H_2$ for 60 min, and the resulted spectra were presented in Fig. 7A. The pair peaks at 1624 and 1343 cm^{-1} nearly vanished in 5 min simultaneously after switching the reaction gas to H_2/Ar, which confirmed the assignment of these two peaks to the same species of monodentate formate. A similar trend of syn-

chronized decrease in intensity was observed for the two bands of bidentate formate at 1603 and 1368 cm^{-1}. Besides, a relatively slower decease of the peaks due to the carbonates family was observed with no appearance of new peaks, suggesting that carbonates species reacted with H_2 to form formate species [37,41–43]. In order to quantitatively compare the change of these two surface formate species mentioned above, the spectra in the range of 1250–1900 cm^{-1} were converted into Kubelka-Munk function and fitted on the basis of the assignments above. The peak areas in the Kubelka-Munk function after the desired time of reaction with H_2/Ar were further defined as A, and the initial areas as A_0. Fig. 7B showed the peak area ratio A/A_0 of 1624 and 1603 cm^{-1} as a function of time-on-stream after exposure to 20% H_2/Ar. Switching the feed gas to H_2 resulted in a significant decrease of approximately 90% monodentate formate species in the first 5 min whereas the peak area of surface bidentate formate species only decreased 50% on the same time scale. After reacting with H_2 for 30 min, the bands of monodentate formate species were decreased by 95% compared to only 60% for the peak at 1603 cm^{-1} of bidentate formate species. These results confirmed that the monodentate formate was more active toward H_2 than the bidentate formate species over $NiWMgO_x$. The W addition in Ni-Mg mixed oxide catalysts unambiguously facilitated the formation of monodentate formate species, which should be a key factor in the enhanced CO_2 methanation activity.

3.7. Characterization results

The XRD patterns of the as-calcined and reduced $NiMgO_x$ and $NiWMgO_x$ samples along with NiO and MgO as references were shown in Fig. 8A. The characteristic reflections at 37.3°, 43.4°, 62.9°, 75.5° and 79.4° for NiO and the reflections at 37.2°, 43.2°, 62.4°, 74.8° and 78.9° for MgO were observed, corresponding to (111), (200), (220), (311) and (222) of the face-centered cubic (fcc) NiO and MgO phase, respectively. Distinct peaks at 37.2°, 43.2°, 62.7°, 75.2° and 79.2° were observed on calcined $NiMgO_x$ and $NiWMgO_x$ and all peaks were located close to or in between the same kind of diffraction peaks of NiO and MgO. For instance, as shown in Fig. 8B, the (220) peak of NiO (62.9°) and MgO (62.4°) shifted towards each other to merge into a single peak at 62.7°, implying the formation of solid solution phase in $NiMgO_x$ and $NiWMgO_x$ [23]. After reduction in a flow of H_2 for 60 min at 500 °C, sharp peaks ascribed to metallic Ni at 44.4° (111), 51.8° (200) and 76.4° (220) appeared and the peaks assigned to Ni-Mg solid solution were still discerned for both catalysts (denoted as $NiMgO_x$-r and $NiWMgO_x$-r, respectively). No peaks assigned to W species were observed in the XRD patterns of $NiWMgO_x$, neither on the calcined sample nor on the reduced one, suggesting that W species were highly dispersed in $NiMgO_x$ matrix in stabilized state. $NiMgO_x$ and $NiWMgO_x$ have been characterized by TEM to show the morphologies. It can be seen that the TEM image of $NiMgO_x$ in Fig. 9A consisted of nanosheets with varying particle sizes, from 15 nm to 35 nm. No appearance of metal particles suggested that a homogeneous Ni-Mg solid solution was formed after the calcination. W addition resulted in a decrease of the size of the nanosheets (~10 nm) with no discernable agglomeration of Ni or W particles, indicating that W has entered the solid solution matrix, as shown in Fig. 9B. Energy-dispersive X-ray (EDX) elemental mapping (Fig. S1) clearly showed that the distribution of Ni and Mg elements was relatively homogeneous in $NiMgO_x$. Similar trends were observed for Ni, W and Mg elements in $NiWMgO_x$ (Fig. S2). These results suggested that the catalysts consisted of metallic Ni particles, dispersed W species and Ni-Mg solid solution support under high-temperature reduction atmosphere after being reduced in H_2 at 500 °C. The spent catalysts after the stability test were calcined in air for 60 min at 500 °C and characterized by XRD. It should be noted that the reflection of (220) peak of $NiMgO_x$-s (62.8°) has slightly shifted closer towards the same diffraction peak of NiO (62.9°), suggesting a possible structural change of the solid solution. As a comparison, the diffraction peaks of $NiWMgO_x$-s remained almost unchanged compared to the fresh catalysts.

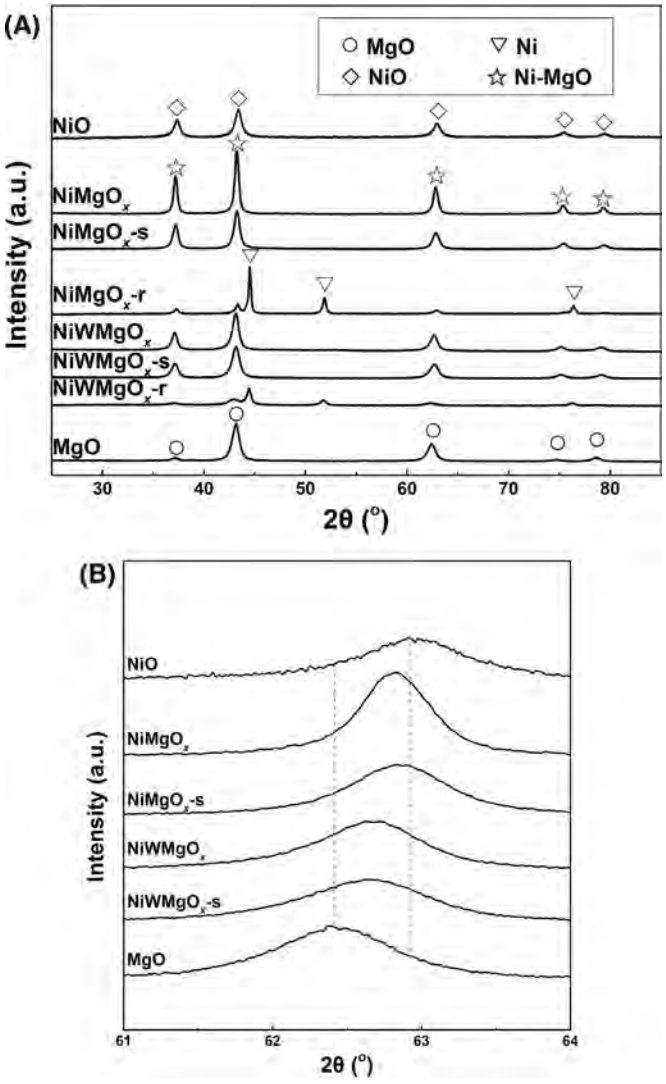

Fig. 8. (A) XRD patterns and (B) enlargement of patterns in the range of 61°–64° for $NiMgO_x$ and $NiWMgO_x$ catalysts. ($NiMgO_x$-s and $NiWMgO_x$-s: The spent catalysts after the stability test were re-calcined in air for 60 min at 500 °C).

As shown in Table 1, similar BET surface areas (about 50 m^2/g) were obtained over as-calcined $NiMgO_x$ and $NiWMgO_x$, whereas a slight decrease (48.94 m^2/g to 45.37 m^2/g) in the surface area was observed on $NiMgO_x$-s catalyst after the stability test. The metallic surface area of both fresh and spent catalysts was determined by H_2 chemisorption after reduction at 500 °C for 60 min, as listed in Table 1. The metallic surface area of $NiMgO_x$-s decreased from 7.01 m^2/g to 3.94 m^2/g after the stability test, compared to the negligible variations for $NiWMgO_x$-s, 7.62 m^2/g–7.55 m^2/g. Inspired by Aziz et al. [25], TGA analysis was carried out under a N_2 flow to estimate the coke content formed during the stability test. The reduced fresh catalysts were studied under the same condition and used as referrences (Fig. S3). The results showed that a 3.8% coke content was formed on $NiMgO_x$-s while the coke formation on $NiWMgO_x$-s was below detectable level.

To further reveal the change of surface properties during the stability test, CO_2-TPD was carried out for the fresh and spent catalysts of both $NiMgO_x$ and $NiWMgO_x$ to determine the basic strength and

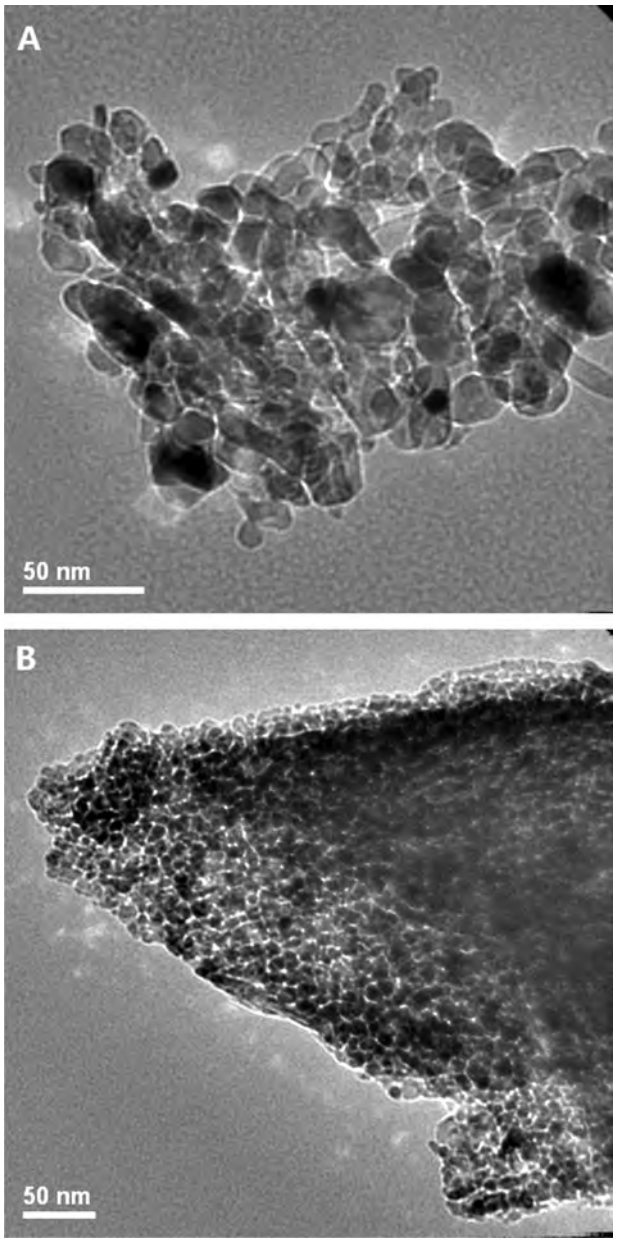

Fig. 9. TEM images of (A) $NiMgO_x$ and (B) $NiWMgO_x$ catalysts.

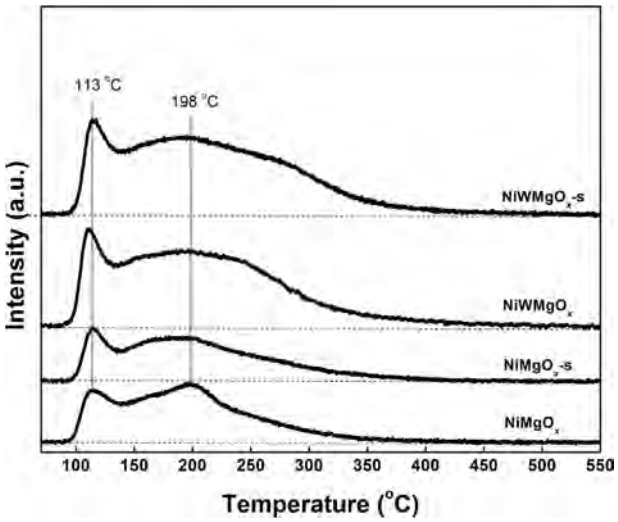

Fig. 10. CO_2-TPD profiles of both fresh and spent $NiMgO_x$ and $NiWMgO_x$ catalysts.

CO_2 adsorption capacity (Fig. 10). For all the catalysts tested, two strong CO_2 desorption peaks, a sharp peak at 113 °C and a broad one centered at 198 °C, were identified. The former peak was attributed to the desorption of CO_2 from weak basic sites, probably Mg sites and unreduced Ni sites on the solid solution support, while the latter one could be assigned to desorption of CO_2 that adsorbed near or on the Ni particles with medium basicity [19,44]. The weak and medium basic sites are both beneficial for the activation of CO_2 while the CO_2 adsorbed on strong basic sites cannot participate in the methanation reaction [37]. *Operando* IR studies over NiUSY zeolites showed that both the CO_2 adsorbed on the weak basic sites of the support and the CO_2 adsorbed on the Ni particles can react with the atomic H to form formate species and further contribute to the production of methane [34]. Similar results were reported by Pan et al. over $Ni/Ce_{0.5}Zr_{0.5}O_2$ [36]. Thus, the total amount of CO_2 adsorption over each sample was estimated from the area under CO_2-TPD peaks and listed in Table 1. The volume of CO_2 desorbed from $NiWMgO_x$ was almost twice of that from $NiMgO_x$, 102.3 μmol/g to 50.9 μmol/g, indicating that W addition prominently increased the amount of surface basic sites. After stability test, the $NiWMgO_x$-s showed almost the same CO_2 adsorption volume as the fresh one, while $NiMgO_x$-s had only 42.5 μmol/g CO_2 uptake compared to 50.9 μmol/g for the fresh $NiMgO_x$ catalyst. Therefore, the W addition not only increased the amount of CO_2 adsorption sites but also remarkably promoted the stability of those sites according to the CO_2-TPD detection.

Fig. 11 displayed the H_2-TPR profiles of both $NiMgO_x$ and $NiWMgO_x$ along with the spent samples in stability test. Prior to the reduction by H_2, samples were *in situ* pretreated in air at 500 °C for 60 min. A prominent H_2 consumption peak at 391 °C was clearly identified for fresh $NiMgO_x$, which was attributed to the reduction of Ni located at the outermost layer of the support [45,46]. The small peak at around 757 °C could be assigned to the reduction of Ni^{2+} located deep in the lattice of the Ni-Mg solid solution [27]. After the stability test, a small shoulder peak appeared at 290 °C over $NiMgO_x$, referring to the reduction of 'unsupported' free NiO, accompanied by the obvious decrease of the area under the peak at 391 °C. The change of H_2-TPR profile of $NiMgO_x$-s indicated that the

Table 1
BET surface area, metallic surface area, coke content and CO_2 adsorption volume of both the fresh and spent catalysts.

Sample	BET surface area (m^2/g)	Metallic surface area[a] (m^2/g)	Coke content[b] (%)	CO_2 adsorption volume[c] (μmol/g)
$NiMgO_x$	48.94	7.01	–	50.9
$NiMgO_x$-s	45.37	3.94	3.8	42.5
$NiWMgO_x$	52.83	7.62	–	102.3
$NiWMgO_x$-s	52.41	7.55	0.0	101.1

[a] Obtained from the H_2 chemisorption results.
[b] Determined from TGA analysis. Calculated as (g of deposits)/(g of calcined sample) × 100%.
[c] Estimated from CO_2-TPD results.

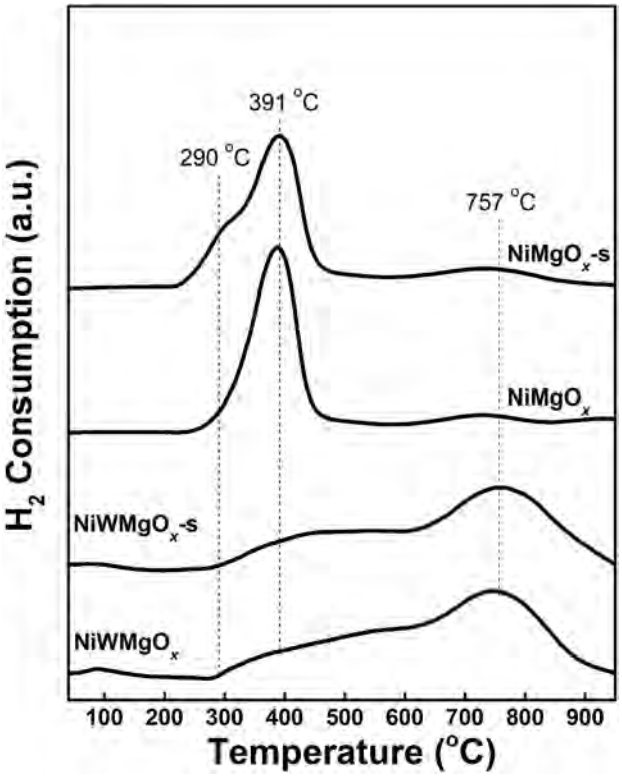

Fig. 11. H_2-TPR profiles of both fresh and spent $NiMgO_x$ and $NiWMgO_x$ catalysts.

Ni species in the outmost layer of the solid solution lost their interaction with the support during the stability test, resulting in the formation of free NiO and probably further sintering of Ni particle, which could be the main cause of the deactivation of $NiMgO_x$ catalysts. The formation of free NiO agreed well with the XRD results of $NiMgO_x$-s. On the other hand, the H_2-TPR profile of fresh $NiWMgO_x$ showed a H_2 consumption bulge between 300–900 °C along with a crest at 757 °C, which ascribed to the reduction of Ni species having different interaction strength with the support of Ni-Mg solid solution. The continuous H_2 consumption at the high temperature region pointed out that a diversity of Ni species were formed as a result of diffusion of NiO into the support after the W addition, from the outmost layer to subsurface layer and then to the deep lattice. It also has been reported that $NiWO_4$ can be formed over Ni-W-Al mixed oxide by calcination at 1000 °C, which can be reduced by H_2 at approximately 800 °C [47]. However, the assignment of the peak at around 757 °C to Ni species located deep in the lattice of the solid solution was well supported by the lack of $NiWO_4$ peaks in the XRD patterns and the fact that a much lower calcination temperature was used in this study. No appearance of new peaks for the $NiWMgO_x$-s indicated that no change occurred in the interaction between Ni and the solid solution support during the stability test for W doped Ni-Mg mixed oxide catalysts.

After being pretreated in H_2 at 500 °C for 60 min, the NiO species in the outmost layer, which less strongly interacted with the support, and NiO species of moderate interaction strength in subsurface layer and a part of NiO species located in deep lattice of Ni-Mg solid solution can be reduced to active metallic Ni [45,48]. The reduction of those NiO species left different amounts of defects in accordance with their interaction strength with the support, which then became the anchoring sites for the Ni particles [28,31]. Compared to the rest two kinds, NiO in the outmost layer with less anchoring sites was more fragile and more sensitive to structure change, as demonstrated by the transformation of this species into free Ni on $NiMgO_x$ after stability test, the sintering of which was responsible for the activity loss.

During the methanation over $NiWMgO_x$ catalysts, CO_2 can adsorb on Mg sites on the solid solution support [11], and probably also Ni sites [34], while H_2 was dissociated on metallic Ni particles [36]. The atomic H then reacted with the adsorbed CO_2 species to form formate species [37]. W doping promoted the formation of active monodentate formate species, leading to an enhanced methanation activity. Furthermore, as shown in the H_2-TPR profiles of $NiWMgO_x$, the addition of W gave rise to an enhancement of the diffusion of NiO into the Ni-Mg solid solution, which increased the anchoring sites for the reduced metallic Ni, resulted in a strong resistance against sintering and a promoted stability of $NiWMgO_x$.

4. Conclusions

The methanation of CO_2 was performed over a novel $NiWMgO_x$ catalyst with W species highly dispersed in Ni-Mg solid solution matrix. Superior catalytic performance with CO_2 conversion of 83% and CH_4 selectivity of 99% was obtained at a low temperature (300 °C). $NiWMgO_x$ catalyst also possessed a great anti-CO-poison ability and a strong resistance against coke formation, demonstrating a long lifetime in the highly exothermic atmosphere of CO_2 methanation, over which indiscernible activity loss was observed during the stability test performed for 100 h either in the presence of 1% CO gas or at a high temperature of 400 °C. *In situ* DRIFTS spectra revealed that the formation of monodentate formate species as active intermediates during CO_2 methanation process was facilitated by W-modified surface with comparison to Ni-Mg mixed oxide catalysts, which subsequently contributed to a significantly enhanced catalytic activity. Moreover, the W species played a critical role in promoting the formation of the surface CO_2 adsorption sites and enhancing their stability, according to CO_2-TPR results. Besides, H_2-TPR demonstrated that, with the aid of W addition, Ni-Mg interaction was strengthened *via* favoring the anchoring of the active Ni species and resistance to their sintering, leading to a largely enhanced stability of $NiWMgO_x$ catalyst.

Acknowledgement

This project is funded by the National Research Foundation (NRF), Prime Minister's Office, Singapore under its Campus for Research Excellence and Technological Enterprise (CREATE) program.

Appendix A. Supplementary data

Supplementary data associated with this article can be found, in the online version, at http://dx.doi.org/10.1016/j.apcatb.2016.05.016.

References

[1] P. Sabatier, J.B. Senderens, CR Acad. Sci. Paris 134 (1902) 514.
[2] S. Tada, R. Kikuchi, Catal. Sci. Technol. 5 (2015) 3061–3070.
[3] Y. Zhu, S. Zhang, Y. Ye, X. Zhang, L. Wang, W. Zhu, F. Cheng, F. Tao, ACS Catal. 2 (2012) 2403–2408.
[4] D. Theleritis, S. Souentie, A. Siokou, A. Katsaounis, C.G. Vayenas, ACS Catal. 2 (2012) 770–780.
[5] A.M. Abdel-Mageed, S. Eckle, R.J. Behm, J. Am. Chem. Soc. 137 (2015) 8672–8675.
[6] C. Swalus, M. Jacquemin, C. Poleunis, P. Bertrand, P. Ruiz, Appl. Catal. B Environ. 125 (2012) 41–50.
[7] A. Karelovic, P. Ruiz, Appl. Catal. B Environ. 113 (2012) 237–249.
[8] A. Beuls, C. Swalus, M. Jacquemin, G. Heyen, A. Karelovic, P. Ruiz, Appl. Catal. B Environ. 113 (2012) 2–10.
[9] J.C. Matsubu, V.N. Yang, P. Christopher, J. Am. Chem. Soc. 137 (2015) 3076–3084.
[10] A. Karelovic, P. Ruiz, ACS Catal. 3 (2013) 2799–2812.

[11] J.N. Park, E.W. McFarland, J. Catal. 266 (2009) 92–97.
[12] A. Erdohelyi, M. Pasztor, F. Solymosi, J. Catal. 98 (1986) 166–177.
[13] N. Takezawa, H. Terunuma, M. Shimokawabe, H. Kobayashib, Appl. Catal. 23 (1986) 291–298.
[14] J. Liu, C. Li, F. Wang, S. He, H. Chen, Y. Zhao, M. Wei, D.G. Evans, X. Duan, Catal. Sci. Technol. 3 (2013) 2627–2633.
[15] M. Agnelli, M. Kolb, C. Mirodatos, J. Catal. 148 (1994) 9–21.
[16] M. Guo, G. Lu, Catal. Commun. 54 (2014) 55–60.
[17] W. Zhen, B. Li, G. Lu, J. Ma, Chem. Commun. 51 (2015) 1728–1731.
[18] G.D. Weatherbee, C.H. Bartholomew, J. Catal. 77 (1982) 460–472.
[19] M. Tan, X. Wang, X. Wang, X. Zou, W. Ding, X. Lu, J. Catal. 329 (2015) 151–166.
[20] T. Nakayama, N. Ichikuni, S. Sato, F. Nozaki, Appl. Catal. A Gen. 158 (1997) 185–199.
[21] F. Arena, B.A. Horrell, D.L. Cocke, A. Parmaliana, N. Giordano, J. Catal. 132 (1991) 58–67.
[22] A. Parmaliana, F. Arena, F. Frusteri, S. Coluccia, L. Marchese, G. Martra, A.L. Chuvilin, J. Catal. 141 (1993) 34–47.
[23] Y. Li, G. Lu, J. Ma, RSC Adv. 4 (2014) 17420–17428.
[24] M.A.A. Aziz, A.A. Jalil, S. Triwahyono, R.R. Mukti, Y.H. Taufiq-Yap, M.R. Sazegar, Appl. Catal. B Environ. 147 (2014) 359–368.
[25] W. Zhen, B. Li, G. Lu, J. Ma, RSC Adv. 4 (2014) 16472–16479.
[26] W.M. Shen, J.A. Dumesic, C.G. Hill Jr., J. Catal. 68 (1981) 152–165.
[27] J. Liu, J. Yu, F. Su, G. Xu, Catal. Sci. Technol. 4 (2014) 472–481.
[28] Y. Wang, H. Liu, B. Xu, J. Mol. Catal. A Chem. 299 (2009) 44–52.
[29] M. Guo, G. Lu, RSC Adv. 4 (2014) 58171–58177.
[30] H. Zhu, R. Razzaq, C. Li, Y. Muhmmad, S. Zhang, AIChE J. 59 (2013) 2567–2576.
[31] Z. Liu, W. Xu, S. Yao, A.C. Johnson-Peck, F. Zhao, P. Michorczyk, A. Kubacka, E.A. Stach, M. Fernández-García, S.D. Senanayake, J.A. Rodriguez, J. Catal. 321 (2015) 90–99.
[32] H. Wu, Y. Chang, J. Wu, J. Lin, I. Lin, C.S. Chen, Catal. Sci. Technol. 5 (2015) 4154–4163.
[33] M.A.A. Aziz, A.A. Jalil, S. Triwahyono, A. Ahmad, Green Chem. 17 (2015) 2647–2663.
[34] A. Westermann, B. Azambre, M.C. Bacariza, I. Graça, M.F. Ribeiro, J.M. Lopes, C. Henriques, Appl. Catal. B Environ. 174–175 (2015) 120–125.
[35] S. Tada, R. Kikuchi, A. Takagaki, T. Sugawara, S.T. Oyama, K. Urasaki, S. Satokawa, Appl. Catal. B Environ. 140–141 (2013) 258–264.
[36] Q. Pan, J. Peng, S. Wang, S. Wang, Catal. Sci. Technol. 4 (2014) 502–509.
[37] Q. Pan, J. Peng, T. Sun, S. Wang, S. Wang, Catal. Commun. 45 (2014) 74–78.
[38] M.R. Prairie, A. Renken, J.G. Highfield, K.R. Thampi, M. Gratzel, J. Catal. 129 (1991) 130–144.
[39] G. Hu, L. Zhu, A. Jia, X. Hu, G. Xie, J. Lu, M. Luo, Appl. Spectrosc. 66 (2012) 122–127.
[40] D. Cornu, H. Guesmi, J.-M. Krafft, H. Lauron-Pernot, J. Phys. Chem. C 116 (2012) 6645–6654.
[41] W. Wang, S.P. Wang, X.B. Ma, J.L. Gong, Chem. Soc. Rev. 40 (2011) 3703–3727.
[42] M. Marwood, R. Doepper, A. Renken, Appl. Catal. A Gen. 151 (1997) 223–246.
[43] S. Tada, O.J. Ochieng, R. Kikuchi, T. Haneda, H. Kameyama, Int. J. Hydrogen Energy 39 (2014) 10090–10100.
[44] S.C. Dantas, J.C. Escritori, R.R. Soares, C.E. Hori, Chem. Eng. J. 156 (2010) 380–387.
[45] A. Parmaliana, F. Arena, F. Frusteri, N. Giordano, J. Chem. Soc. Faraday Trans. 86 (1990) 2663–2669.
[46] Q. Liu, J. Gao, M. Zhang, H. Li, F. Gu, G. Xu, Z. Zhong, F. Su, RSC Adv. 4 (2014) 16094–16103.
[47] D.W. Southmayd, C. Contescu, J.A. Schwarz, J. Chem. Soc. Faraday Trans. 89 (1993) 2075–2083.
[48] S. Takenaka, S. Sato, R. Takahashi, T. Sodesawa, Phys. Chem. Chem. Phys. 5 (2003) 4968–4973.